Evolution of Discontinuous/Continuous $Al_3(Sc,Zr)$ Precipitation in Al-Mg-Mn 5083 Alloy during Thermomechanical Process and its Impact on Tensile Properties

Ahmed Y. Algendy [1], Kun Liu [1,*], Paul Rometsch [2], Nick Parson [2], X.-Grant Chen [1,*]

[1] Department of Applied Science, University of Quebec at Chicoutimi, Saguenay (QC), G7H 2B1, Canada
[2] Arvida Research and Development Center, Rio Tinto Aluminum, Saguenay (QC), G7S 4K8, Canada

*Corresponding authors: kun.liu@uqac.ca and xgrant_chen@uqac.ca

Abstract

The evolution of discontinuous and continuous $Al_3(Sc,Zr)$ precipitation in an Al-Mg-MnAA5083 alloy during heat treatment and hot rolling was investigated. The results showed that, at a high Sc content (0.43 wt.%), a large number of line/fan-shaped structures were formed as discontinuous $Al_3(Sc,Zr)$ precipitation during solidification, while no such discontinuous precipitation was observed when the amount of Sc added was low (0.15 wt.%). During the three-step heat treatment (275 °C /12 h + 375 °C/48 h + 425 °C/12 h), two types of precipitates — Mn-bearing dispersoids and spherical $Al_3(Sc,Zr)$ precipitates — were formed as the main strengthening phases. In the high-Sc alloy, the discontinuous $Al_3(Sc,Zr)$ precipitates dissolved partially. However, the quantity of the spherical $Al_3(Sc,Zr)$ precipitates in the high-Sc alloy was much lower than that in the low-Sc alloy, which degraded its aging hardening response. During hot rolling, although the discontinuous precipitates were completely dissolved, the number density of the spherical $Al_3(Sc,Zr)$ precipitates in the high-Sc alloy was still lower than that in the low-Sc alloy. The tensile properties of the Sc-containing alloys improved significantly compared with those of the base alloy. However, the yield and ultimate tensile strengths of the high-Sc alloy were lower than those of the low-Sc alloy. This indicates that the discontinuous precipitation had a deleterious effect on the mechanical properties of the alloy.

Keywords: Al-Mg-Mn 5083 alloy, Discontinuous $Al_3(Sc,Zr)$ precipitation, Sc and Zr addition, Microstructure, Mechanical properties.

1. Introduction

Microalloying of rare-earth elements, especially Sc, is an efficient approach to improving the mechanical properties of aluminum and its alloys [1-3]. Microalloying with Sc can significantly improve the mechanical properties, preserve the work hardening and enhance the recrystallization resistance of Al-Mg-Mn 5xxx alloys [4-6]. In Sc-containing alloys, a high number of fine and

coherent $L1_2$-Al_3Sc particles can be precipitated in the aluminum matrix as the strengthening phase through the decomposition of the supersaturated solid solution during aging treatment at relatively high temperatures [4, 7-10]. Owing to its cost-effectiveness, Zr is often added together with Sc. Zr can substitute Sc in Al_3Sc and form core-shell $Al_3(Sc_{1-x},Zr_x)$ precipitates with the same $L1_2$-crystal structure while improved coarsening resistance [11, 12].

In Al-Sc/Al-Sc-Zr systems, Al_3Sc/Al_3(Sc, Zr) precipitates are formed continuously and discontinuously [13-16]. Continuous precipitation usually occurs during aging treatment (300–425 °C). Nano-sized Al_3Sc/Al_3(Sc,Zr) precipitates effectively retard the dislocation and grain boundary movements and significantly improve the alloy properties [4, 8, 9, 11]. However, discontinuous precipitation can also occur during solidification or aging treatment [16-19]. The tendency of Al-Sc alloys to form Al_3Sc discontinuous precipitates is strongly related to their Sc level (often in high-Sc hypereutectic alloys) [14, 16, 20, 21], solidification rate [14, 17, 18, 22], and annealing temperature [14, 19]. Norman *et al.* [20] reported that the discontinuous precipitation reaction of rod-like precipitates occurs during solidification cooling to room temperature in a hypereutectic 0.79 wt.% Sc alloy. According to Black and Hopkins [21], discontinuous Al_3Sc precipitates with various morphologies, including rod- and branch-like morphologies, can be formed during the solidification of Al-1.0 wt.% Sc. Furthermore, the effect of the cooling rate during solidification on the Al_3Sc discontinuous precipitation of Al-Sc alloys has been investigated [17, 22]. The results reported the formation of rod- and lamellae-shaped Al_3(Sc,Zr) precipitates at slow cooling rates and a decrease in the number density of these precipitates with the increasing cooling rate. Lathabai *et al.* [18] reported that discontinuous precipitation in the as-cast microstructure of Al-4.5%Mg-0.7Mn alloy occurs within a low range of 0.17–0.26 wt.% Sc. Similar discontinuous precipitation phenomena have been observed in other alloy systems containing transition metals, such as Al-Zr [23] and Al-Li [24].

Most studies related to the effect of discontinuous precipitation on the mechanical properties of Al-Sc/Al-Sc-Zr systems considered Al_3Sc discontinuous precipitates as an undesirable microstructure, which negatively affects the mechanical properties of the alloy. Zhang *et al*. [19] reported the deterioration effect of discontinuous precipitates on the microhardness of heat-treated Al-0.7 wt.% Sc. Lohar *et al.* [22] observed that the as-cast Al_3(Sc,Zr) discontinuous precipitates in an Al-0.3Sc-0.15Zr alloy lowered its microhardness during aging. However, Lathabai *et al.* [18] found that the microhardness and tensile properties of an Al-4.5%Mg-0.7Mn alloy with 0.17% Sc addition increased compared to those of the Sc-free counterpart despite the occurrence of discontinuous precipitation.

To date, studies on the effect of discontinuous/continuous precipitation of Al_3(Sc,Zr) precipitation on the mechanical properties of Al-Mg-Mn alloys have been scarce, and most of them focused on the microstructural evolution of Al_3(Sc,Zr) discontinuous precipitates. This study investigated the precipitation behaviors of discontinuous and continuous precipitates in a typical Al-Mg-Mn 5083 alloy with various Sc levels during the thermomechanical process (heat treatment

and hot rolling). The effect of discontinuous precipitation on the aging response and tensile properties of the hot-rolled sheets was also studied.

2. Experimental Procedure

Three Al-Mg-Mn alloys were prepared according to the typical AA5083 chemical composition. The chemical compositions of experimental alloys analyzed with optical omission spectrometer are listed in Table 1. In addition to the base alloy , the alloy L-Sc contained 0.16% Sc and 0.17% Zr, and the alloy H-Sc had 0.43% Sc and 0.15% Zr (all the alloy compositions used in this study were in wt.%). The alloys were batched in a graphite crucible using an electric resistance furnace at 780 ^{o}C. After melting and degassing, the melt was poured into a permanent steel mold preheated at 250 ^{o}C, which had a cooling rate of ~2 ℃/s during solidification. The dimensions of the cast ingots were 30 × 40 × 80 mm.

Table 1 Chemical composition of experimental alloys (wt.%)

Alloys	Mg	Mn	Si	Fe	Cu	Cr	Ti	Sc	Zr
Base	4.78	0.79	0.26	0.31	0.12	0.14	0.09	---	---
L-Sc	4.75	0.80	0.30	0.31	0.11	0.15	0.09	**0.16**	**0.17**
H-Sc	4.76	0.75	0.30	0.33	0.10	0.15	0.10	**0.43**	**0.15**

A three-step heat treatment (275^{o}C/12h + 375^{o}C/48h + 425^{o}C/12h) was applied to all cast ingots to promote the effective precipitation of Mn-bearing dispersoids and Al_3(Sc,Zr) precipitates in the aluminum matrix [25]. The heat treatment was conducted in a programmable electric air circulating furnace with a 60 ^{o}C/h heat rate. The thickness of the heat-treated ingots was machined to 26.5 mm, and then preheated at 500 ℃ for 1.5 h prior hot rolling. The ingots were hot-rolled in multiple passes at a temperature of 500±10 ℃. The thickness reduction of each pass is approximately 3.2 mm. The rolled plate was back to the furnace and heated at 500 ℃ for 20 min after each 3 passes to keep rolling at similar temperature. The final thickness of sheet is ~3.2 mm, which is ~ 88% reduction. Prior mechanical testing, all rolled sheets were annealed at 300 ℃ for 5 h to relieve the rolling-induced thermal stress.

The precipitation behavior of precipitates during heat treatment was evaluated by electrical conductivity (EC) and microhardness (HV) measurements. EC was deterimined using a sigmascope SMP 10 electrical conductivity device with a %IACS unit at room temperature. Vickers microhardness was obtained using NG-1000 CCD microhardness machine with 25 g load for 20 s dwelling time. Generally, 20 measurements were performed to evaluate the average hardness value for each sample. The tensile samples were machined according to ASTM E8/E8M-16a in the rolling direction with a gauge size of 3 x 6 mm. Uniaxial tensile tests were conducted

using Instron 8801 servo-hydraulic testing unit at strain rate 0.001 s^{-1}. Average results were obtained from three repeated tests.

The samples were ground and polished using a standard metallographic precedure for microstructure observations. The microstructure of studied alloys was charaterized using optical microscopy (Nikon, Eclipse ME600), scanning electron microscope (SEM, JSM-6480LV) and transmission electron microscope (TEM, JEM-2100). The as-cast, heat-treated and hot-rolled ssamples were observed after etching by 0.5% HF for 30 s. TEM was used to observe the distribution of Mn-bearing dispersoids and Al_3(Sc,Zr) precipitates. All TEM images were taken along the $[001]_{Al}$ zone axis. Centered superlattice dark-field micrograph was recorded along [100] reflections close to <011> direction to reveal Al_3(Sc, Zr) precipitates. The size and number density of precipitates were measured using ImageJ image analysis software with TEM images. The quantitative analysis was performed on 10 images, and each image contains more than 300 particles. The number density of precipitates was determined using the following equation:

$$ND = \frac{N}{A*(D+t)} \qquad (1)$$

Where; N is the number of particles in the TEM image, A is the total area, D is the equivalent diameter, and t is the thickness of the TEM foil, which was measured using the convergent electron beam diffraction (CBED) method [26].

3. Results and discussion

3.1 As-cast microstructure

Fig. 1 shows the as-cast microstructure of the experimental alloys under the optical bright and dark-field modes after etching with Keller's reagent. The as-cast microstructure mainly consisted of α-Al dendrite cells as the matrix, with several intermetallic phases distributed along the dendrite boundaries. The major intermetallic compounds (IMCs) in the three alloys were Fe/Mn-rich α-$Al_{15}(Fe,Mn,Cr)_3Si_2$ and Al_6(Fe,Mn,Cr) intermetallics and primary Mg_2Si intermetallics, as indicated by the SEM-EDS results. In the Sc-containing alloys (low-Sc (L-Sc) and high-Sc (H-Sc)), few primary Al_3(Sc,Zr) particles with cubic morphology were detected in the aluminum dendrite cells (see the inserts in Figs. 1b and 1c).

A noticeable difference was observed in the microstructure of the as-cast alloy after the addition of high Sc (0.43 %). In the aluminum dendrite cells, many areas showed the formation of a line-or fan-shaped structure (Figs. 1c and 1d). This type of precipitation was not easily observed using optical microscopy when the sample was just polished. After etching the H-Sc alloy in the dark-field mode, both line- and fan-shaped Sc-containing particles could be observed (Fig. 1d), which initiated at the dendrite boundaries and extended into the cell interiors. This discontinuous precipitation of Sc-containing particles was related to the decomposition of the saturated solid

solution in the aluminum matrix to form $Al_3(Sc,Zr)$ at a moving grain boundary with a common lamellar structure [21, 27]. In the L-Sc alloy, such discontinuous precipitation rarely occurred.

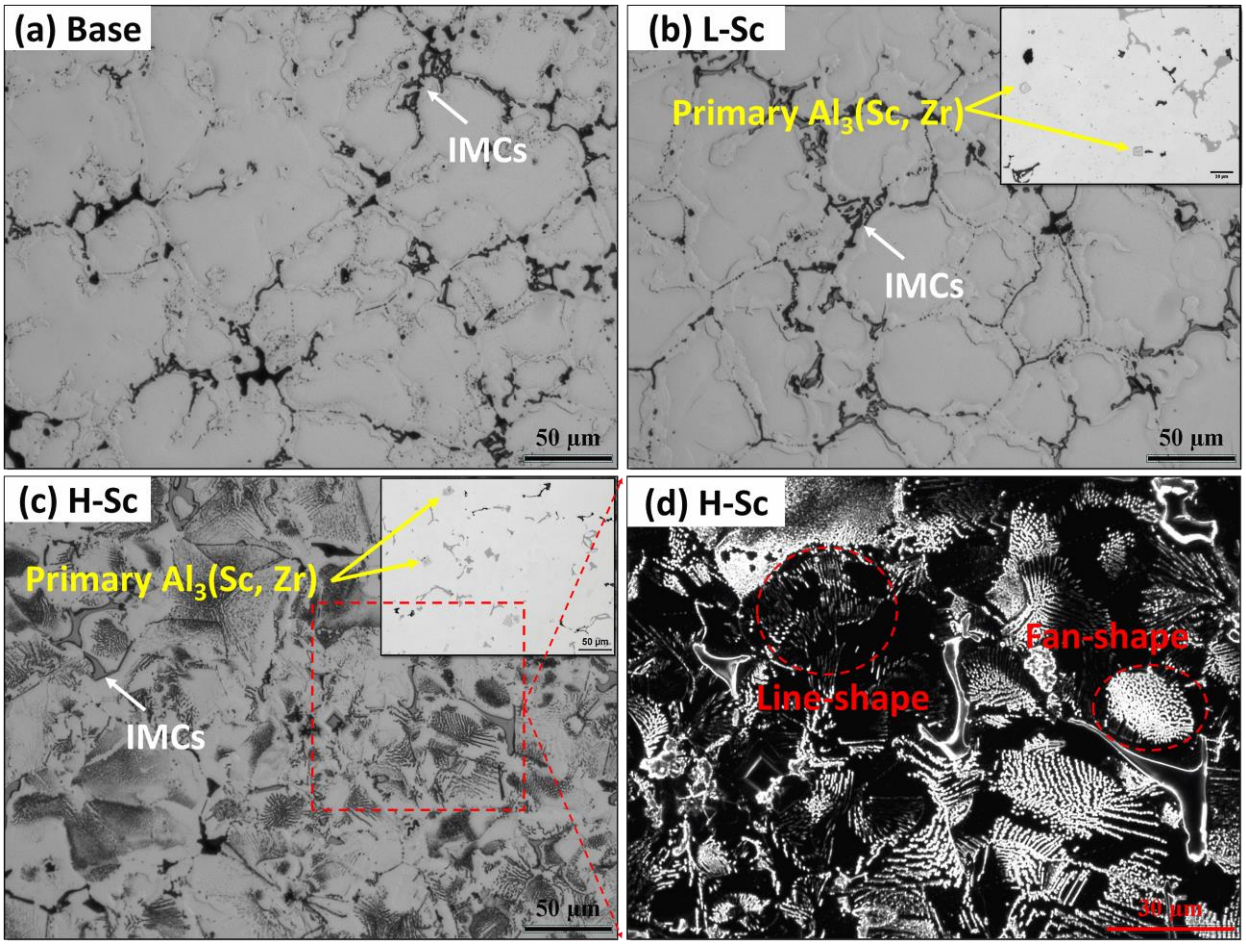

Figure 1: Optical microscopy images of the as-cast microstructure in the bright-field mode after etching with Keller's agent (a) base, (b) L-Sc, and (c) H-Sc alloys. (d) high-magnification dark-field image of the H-Sc alloy showing line/fan-shaped discontinuous precipitation at the dendrite cells. Inserted image in Fig. 1b and c shows the primary $Al_3(Sc,Zr)$.

The discontinuous precipitation in the H-Sc alloy was investigated in detail using TEM, and the results are shown in Fig. 2. The observations were conducted along the $[001]_{Al}$ and $[011]_{Al}$ zone axes. The dark-field TEM images (Figs. 2a and 2b) showed lamellar aggregations near the cell/grain boundaries, which contained a high density of branched and rod-like precipitates. The corresponding selected area diffraction patterns (SADP) along the $[001]_{Al}$ zone axis showed light spots corresponding to the precipitates between the bright α-Al spots (Figs. 2c and 2i). This observation along with the TEM-EDS results (Fig. 2f) confirmed that these precipitates were $L1_2$-$Al_3Sc/Al_3(Sc,Zr)$ [16, 17]. In addition, the orientation relationship between α-Al and the precipitates was observed to be [100]α-Al//[100] precipitates.

Figs. 2d and 2e indicate that the discontinuous precipitation resulted from the multiplication of rod-like precipitates originating at the dendrite cell/grain boundaries, which extended into the dendritic cells. Many rod-like precipitates were aligned in sequence and gave a line-shaped appearance, as indicated by the optical microscopy images (Fig. 1d). This is consistent with the results reported in the literature [16, 23, 28]. In addition, a coarse, spherical $L1_2$-precipitate with a size of 20–30 nm was observed on one end of each rod-like precipitate (yellow circles in Fig. 2e), suggesting that the discontinuous precipitates could nucleate heterogeneously on the pre-existing particles. Mochugovskiy *et al.* [29] found that a line of coarse $L1_2$-dispersoids was formed heterogeneously on the grain boundaries before the onset of discontinuous precipitation. The rod-like precipitates were of different sizes with a length ranging from 500 to 860 nm (Figs. 2d and 2e). Furthermore, the TEM observations (Figs. 2g and 2h) along the $[011]_{Al}$ zone axes confirmed that the rod-like precipitates were aligned in a line sequence.

The formation of discontinuous $Al_3Sc/Al_3(Sc,Zr)$ precipitates during solidification with line- and fan-shaped aggregates has been reported in previous studies [27, 29-32]. Since the casting and solidification conditions of the two Sc-containing alloys were the same, the primary reason for the formation of discontinuous precipitates in the H-Sc alloy was its high Sc level. Hornbogen [30] reported that discontinuous precipitates tend to nucleate heterogeneously along the grain boundaries rather than within the grain interior. During solidification, Sc tends to segregate toward the dendrite boundaries, which are considered fast channels for the redistribution and transportation of solute atoms, enhancing the growth of discontinuous precipitates. Marquis *et al.* [31] reported that the dislocation lines and networks formed owing to internal stress relaxation can also act as heterogeneous nucleation sites for discontinuous Al_3Sc precipitation.

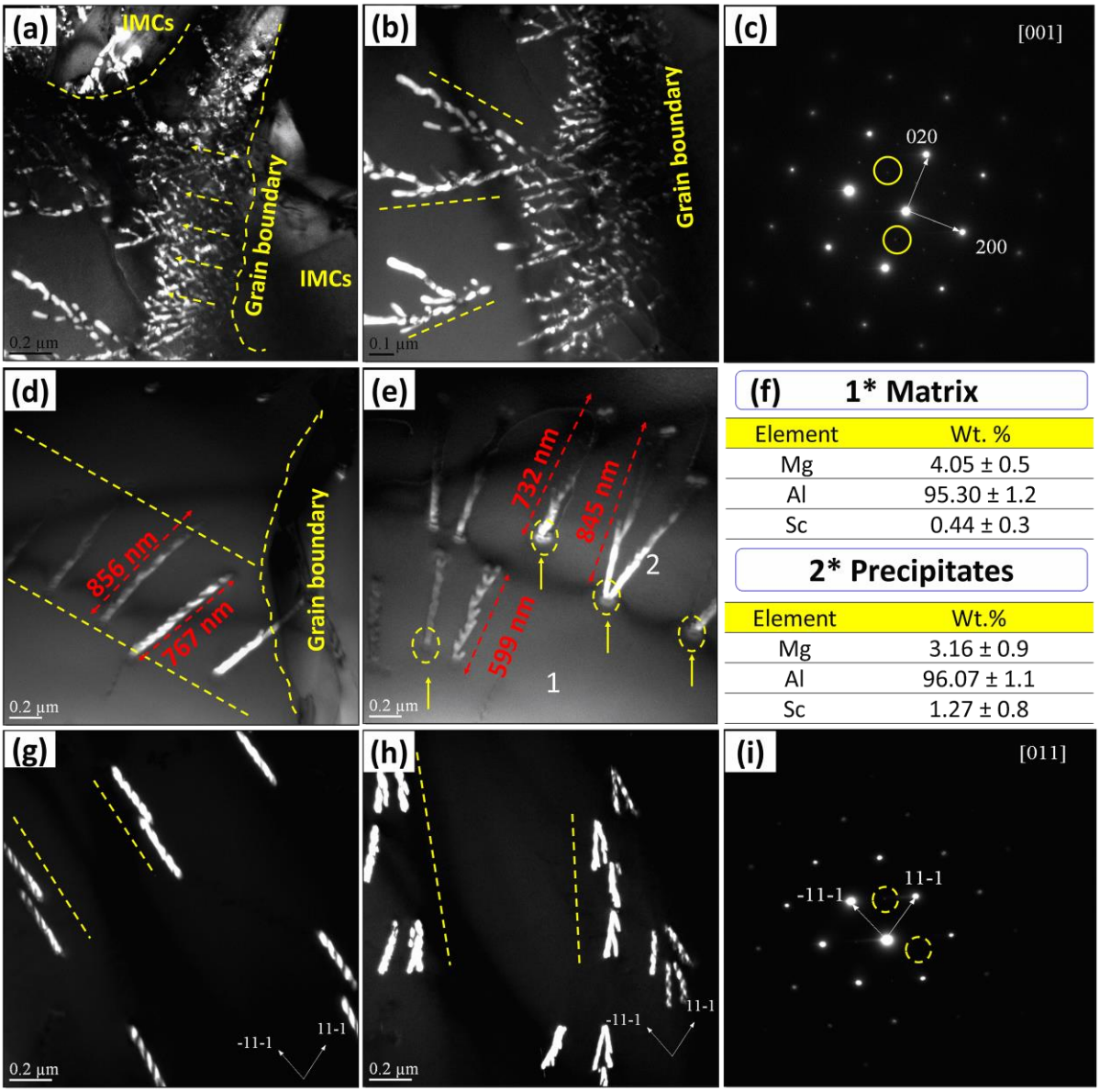

Figure 2: Dark-field TEM images showing the discontinuous precipitation of the H-Sc alloy under the as-cast condition along the (a and b) $[001]_{Al}$, (d and e) $[001]_{Al}$, and (g and h) $[011]_{Al}$ zone axes; (c and i) the corresponding SADPs confirming the $L1_2$-$Al_3Sc/Al_3(Sc,Zr)$ crystal structure of the precipitates; (f) TEM-EDS analysis results showing the chemistry of the matrix and rod-like precipitates.

3.2 Microstructure after heat treatment

Owing to the high Mn content in all the three experimental alloys, Mn-bearing dispersoids precipitated in the aluminum matrix after the three-step heat treatment [25]. The optical microscopy images of the three alloys (Fig. 3a–3c) revealed the presence of a precipitation zone (gray zone marked by the red line) and a precipitate-free zone (PFZ) (bright zone marked by the blue line) in the interdendritic region. The SEM images showed that a large number of Mn-bearing

dispersoids existed in the base and L-Sc alloys (Fig. 3d), whereas the line/fan-shaped structure remained in the H-Sc alloy along with several Mn-bearing dispersoids (Fig. 3e). However, as compared to the as-cast microstructure of the H-Sc alloy (Fig. 1c), the number of line/fan-shaped structures reduced remarkably after the heat treatment process, which indicates that the discontinuous precipitates dissolved partially during the heat treatment process [13, 16].

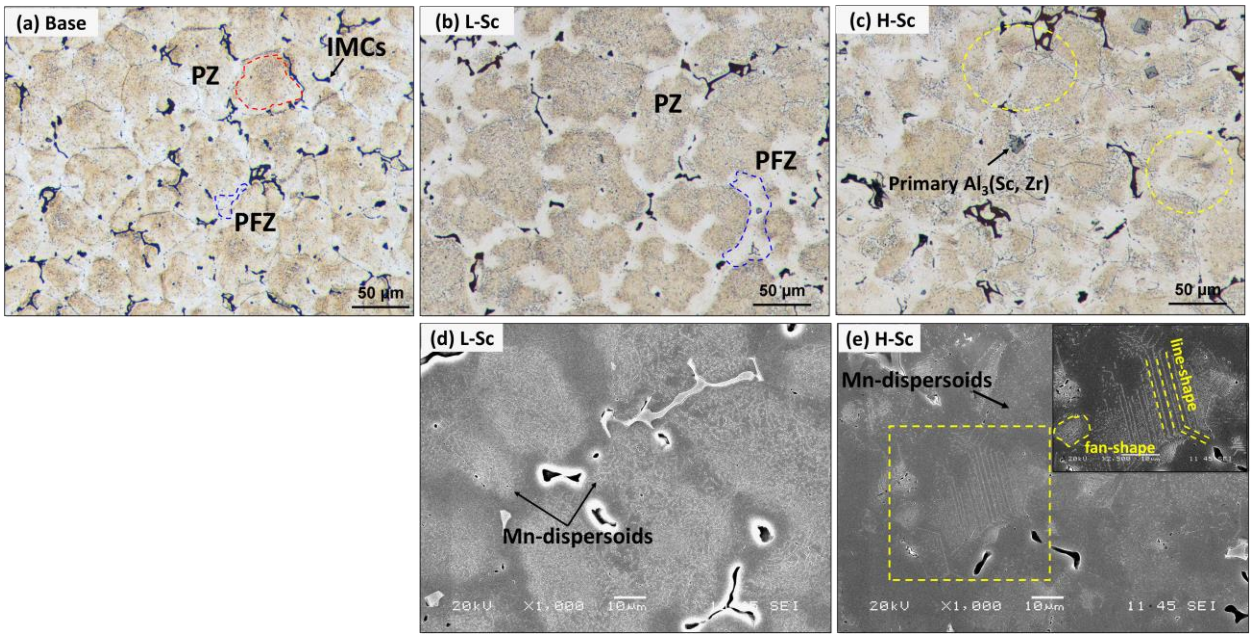

Figure 3: Microstructures of the alloys after the heat treatment showing the distribution of the precipitation zone and precipitate free zone, (a) base alloy, (b) L-Sc and (c) H-Sc alloys. SEM images showing the precipitation of Mn-bearing dispersoids in (d) L-Sc and (e) H-Sc co-existing with the line/fan-shaped structure.

The TEM images provided more details on the precipitation of both the Mn-bearing dispersoids and nano-sized $Al_3(Sc,Zr)$ precipitates during the heat treatment. In the L-Sc alloy, in addition to the Mn-bearing dispersoids (Fig. 4a), a large number of spherical and nano-sized $Al_3(Sc,Zr)$ precipitates were formed in the aluminum matrix (as continuous precipitation (CP)). These precipitates overlapped with the Mn-bearing dispersoids (Fig. 4b). In the H-Sc alloy, a large number of discontinuous rod-like $Al_3(Sc,Zr)$ precipitates (DCP) were widely existed after the precipitation of the Mn-bearing dispersoids and spherical $Al_3(Sc,Zr)$ precipitates. It should be mentioned that the Mn-bearing dispersoids formed in the matrix were Al_4Mn and Al_6Mn disperoids, identified by the selected area diffraction pattern and TEM-EDS analysis (not showing here) [25]. Figs. 4c–4f show two examples of discontinuous rod-like precipitates formed at different locations. The rod-like precipitates were non-uniformly distributed in the aluminum matrix and were much larger than the spherical ones (Fig. 4g). After heat treatment, the size of the rod-like precipitates decreased, and the length ranged from 200 to 350 nm. This indicates that these precipitates dissolved partially in the Al matrix during the heat treatment [16, 33, 34].

Moreover, in the vicinity of the rod-like precipitates, there were almost no spherical and fine $Al_3(Sc,Zr)$ precipitates (indicated by the blue line area), as shown in Fig. 4f. In addition, although the Sc content of the H-Sc alloy was high, it consisted of fewer spherical $Al_3(Sc,Zr)$ precipitates (Fig. 4f) than the L-Sc alloy (Fig. 4b). For instance, the number density of the spherical $Al_3(Sc,Zr)$ precipitates in the H-Sc alloy was 5188 μm^{-3}, while that in the L-Sc alloy was 19700 μm^{-3}. It is evident that the discontinuous precipitates consumed large amounts of Sc and Zr solutes and caused a large decrease in the Sc content in the solid solution, reducing the number density of the spherical $Al_3(Sc,Zr)$ precipitates formed during the subsequent heat treatment process. In addition, it created a depletion area around the rod-like precipitates, making the further precipitation of the spherical $Al_3(Sc,Zr)$ precipitates impossible.

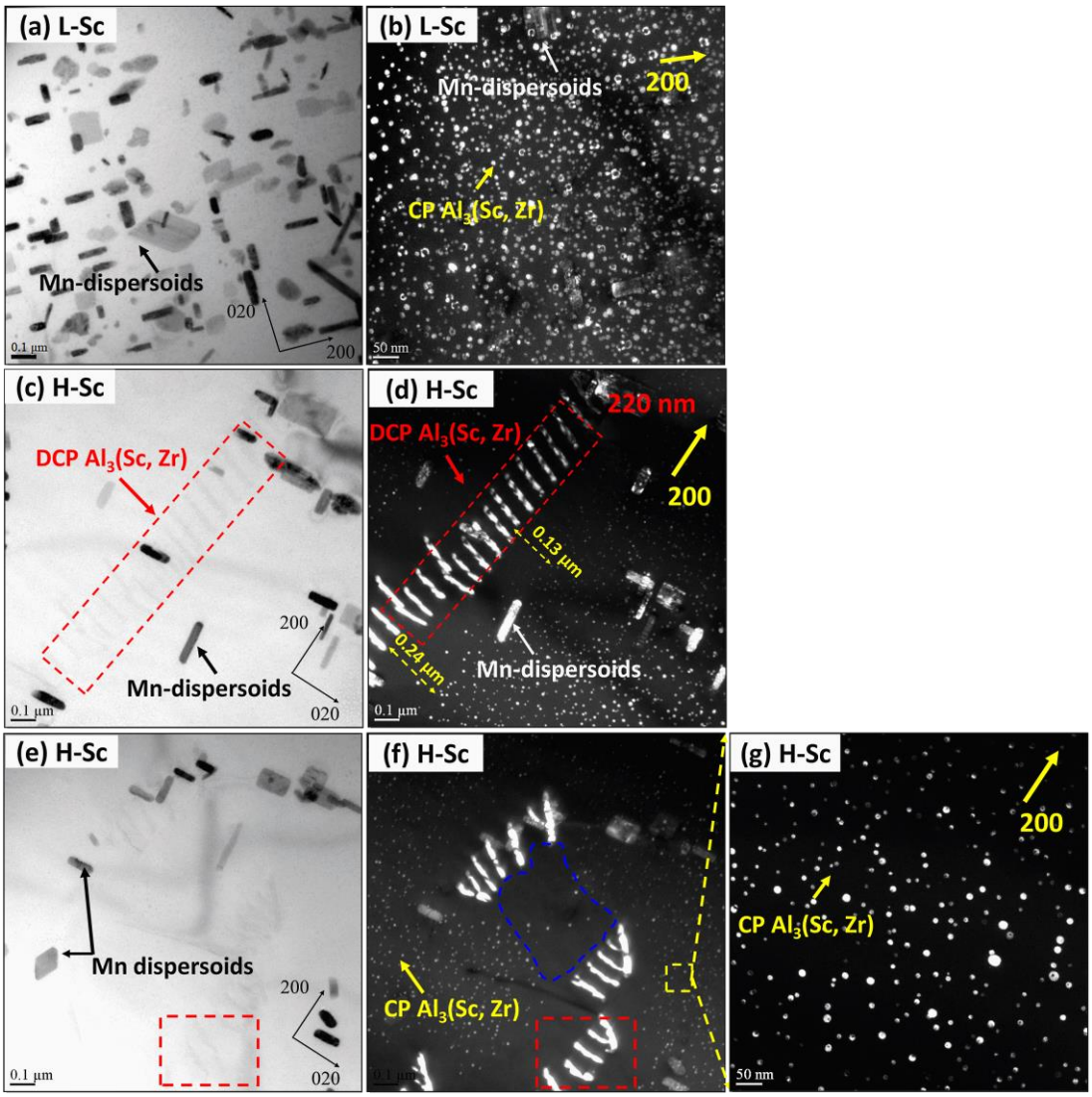

Figure 4: Bright-field (a, c, e) and corresponding dark-field (b, d, f, g) TEM images along the $[001]_{Al}$ zone axis showing the precipitation of Mn-bearing dispersoids, continuous and discontinuous $Al_3(Sc,Zr)$ precipitates in Sc-containing alloys under the heat-treated condition, (a, b) L-Sc and (c–g) H-Sc alloys.

Fig. 5 shows the electrical conductivity and microhardness of the alloys after the heat treatment. Owing to the solid solution effect of Sc and Zr solutes, the electrical conductivity values of the Sc-containing alloys (L-Sc and H-Sc) were slightly lower than those of the base alloy. However, the microhardness values of the Sc-containing alloys were considerably higher than that of the base alloy, which indicates that the nano-sized $Al_3(Sc,Zr)$ precipitates provided a substantial strengthening effect to the alloy. For instance, the microhardness increased from 112 HV for the base alloy to 136.4 HV for the L-Sc alloy. This is because a large number of fine $Al_3(Sc,Zr)$ precipitates coexisted with Mn-bearing dispersoids in the L-Sc alloy. However, the microhardness of the H-Sc alloy was lower (122 HV) than that of the L-Sc alloy (136.4 HV). This indicates that the discontinuous precipitates had a deleterious effect on the precipitation of fine $Al_3(Sc,Zr)$ precipitates, and hence on the hardening response of the alloy.

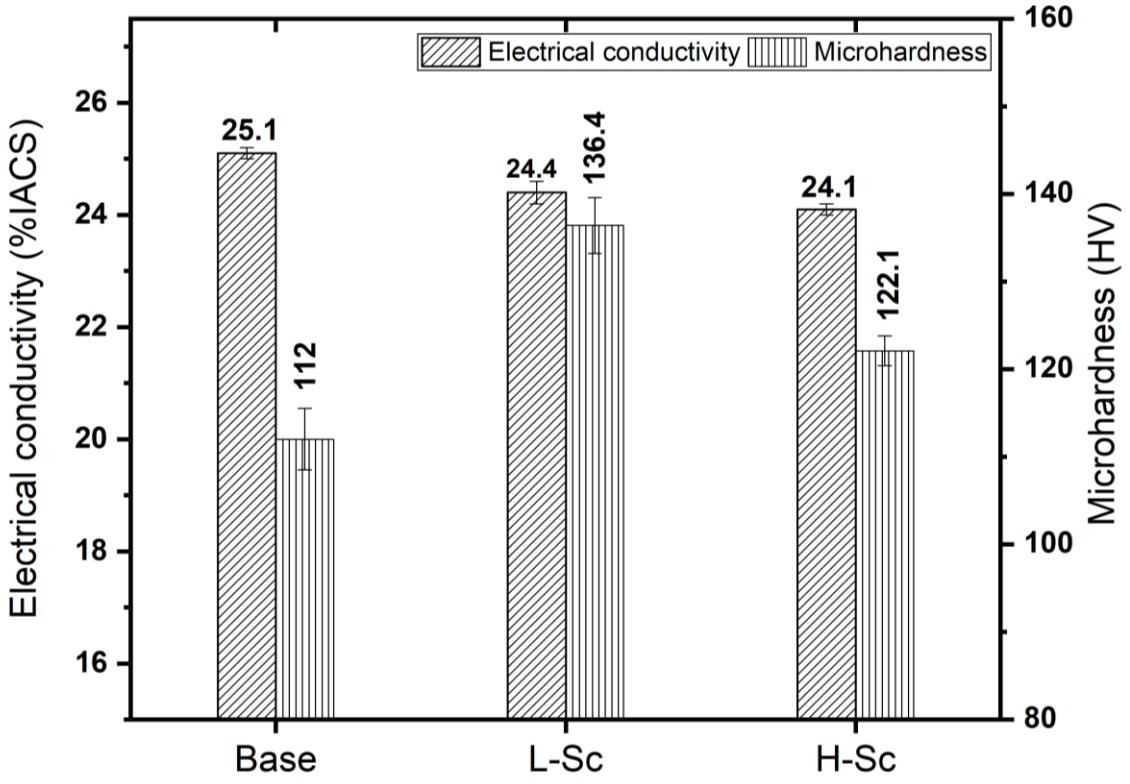

Figure 5: Electrical conductivity and microhardness of the experimental alloys after the heat treatment.

3.3 Microstructure evolution during hot rolling

Prior to rolling, the heat-treated ingots were preheated at 500 °C for 1.5 h to improve their rollability. Fig. 6 shows the microstructure of the preheated sample of the H-Sc alloy. As shown in the figure, some areas with a line-shaped structure (Fig. 6a, marked with yellow circles and Fig. 6b, marked with yellow dashed lines), similar to that observed in the heat-treated sample (Fig. 3), were present in the microstructure. However, these areas were much smaller than those in the heat-

treated sample. In addition, the fan-shaped structure almost disappeared (Fig. 6b). The dark-field TEM image (Fig. 6c) showed the co-existence of rod-like discontinuous precipitates with spherical $Al_3(Sc,Zr)$ precipitates and Mn-bearing dispersoids. As compared to the case of the heat-treated sample (Fig. 4c), in the preheated sample, the size of the rod-like precipitates decreased, and the length ranged from 100 to 250 nm, indicating the further dissolution of the rod-like precipitates during the preheating process at 500 °C. This phenomenon can be explained by the increase in the diffusivity of Sc with increasing temperature [35] and grain boundary stability [36]. Marquis *et al.* [31] reported that rod-like precipitates re-dissolve into the Al matrix during annealing. Sun *et al.* [16] reported the reduction in and disappearance of rod-like precipitates with increasing aging time up to 24 h at 340 °C. In contrast, the spherical $Al_3(Sc,Zr)$ precipitates (Fig. 6d) grew moderately, and their size increased during the preheating process at 500 °C [37, 38].

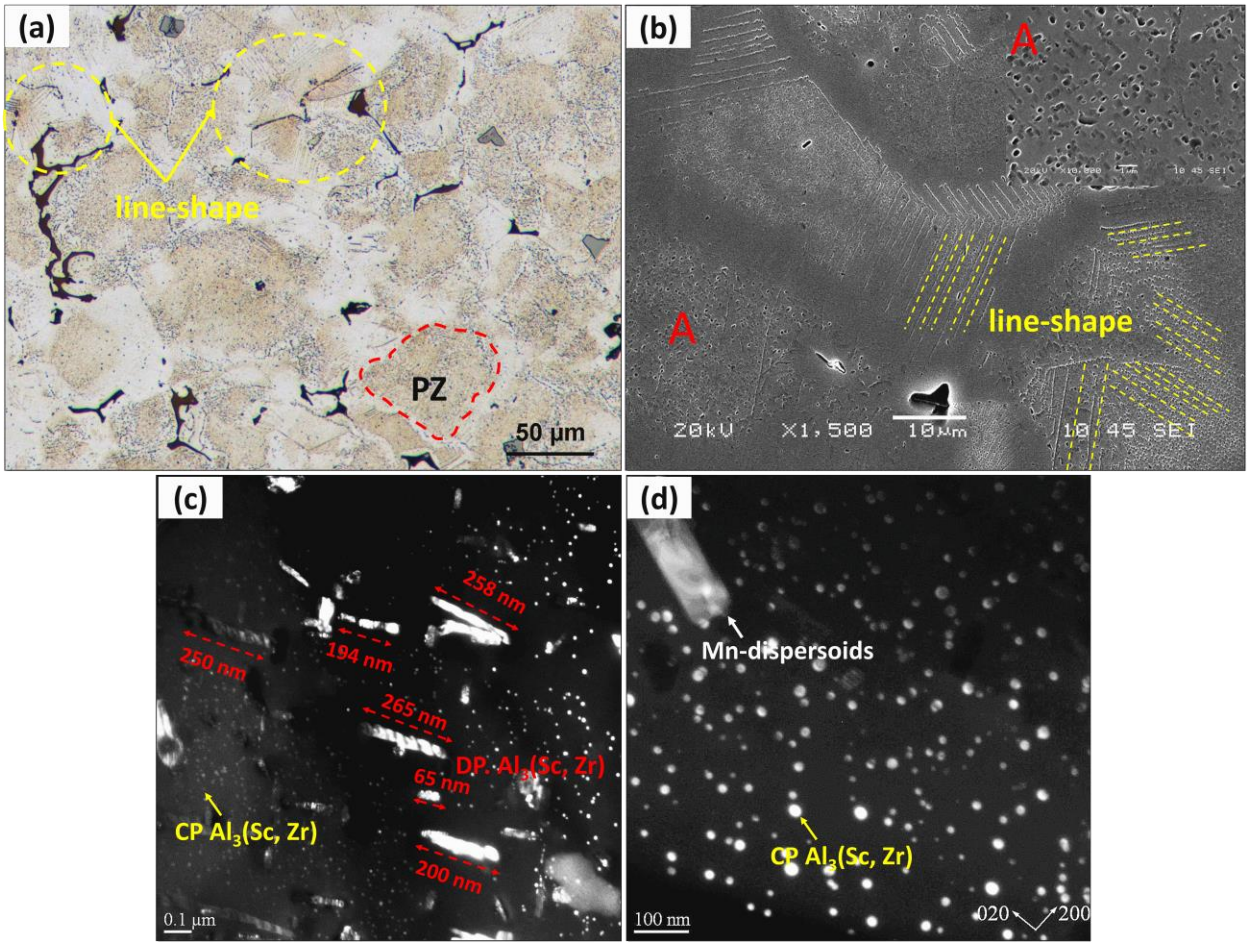

Figure 6: Microstructure of the preheated H-Sc sample (500°C/1.5h), (a) optical microscopy image and (b) SEM image showing the distribution of the line-shaped structure, and (c, d) dark-field TEM images showing the rod-like discontinuous precipitates and spherical $Al_3(Sc,Zr)$ precipitates.

Fig. 7 shows the typical microstructures of the hot-rolled Sc-containing alloys (L-Sc and H-Sc). Both the samples showed elongated grains parallel to the rolling direction (Figs. 7a and 7d), marked by red lines). Moreover, as shown in Fig. 7d, the previous line-shaped structure after

preheating could not be observed after hot rolling. This can be attributed to the accelerated dissolution of the rod-like precipitates with the interaction of the dislocations generated during high-temperature deformation (500 °C) [38-40]. The dark-field TEM images (Figs. 7b and 7c, 7e and 7f) revealed that the spherical $Al_3(Sc,Zr)$ precipitates underwent coarsening in both the alloys during hot rolling, and the number density of these precipitates decreased and the size increased as compared to those of the precipitates observed after the heat treatment (Fig. 4). For instance, in the case of the L-Sc alloy, the number density of the spherical $Al_3(Sc,Zr)$ precipitates decreased from 19700 μm^{-3} (after the heat treatment) to 5695 μm^{-3} after hot rolling while in the case of the H-Sc alloy, it decreased from 5188 μm^{-3} to 650 μm^{-3}. The spherical $Al_3(Sc, Zr)$ precipitates in the L-Sc sample had a much higher number density and significantly smaller size than those in the H-Sc sample. For example, the average diameter of the spherical $Al_3(Sc, Zr)$ precipitates in the L-Sc sample was 12.7 nm while that of the precipitates in the H-Sc sample was 37.8 nm. This indicates that the complete dissolution of the rod-like discontinuous precipitates during hot rolling could not prevent their negative effect on the characteristics of the spherical $Al_3(Sc,Zr)$ precipitates.

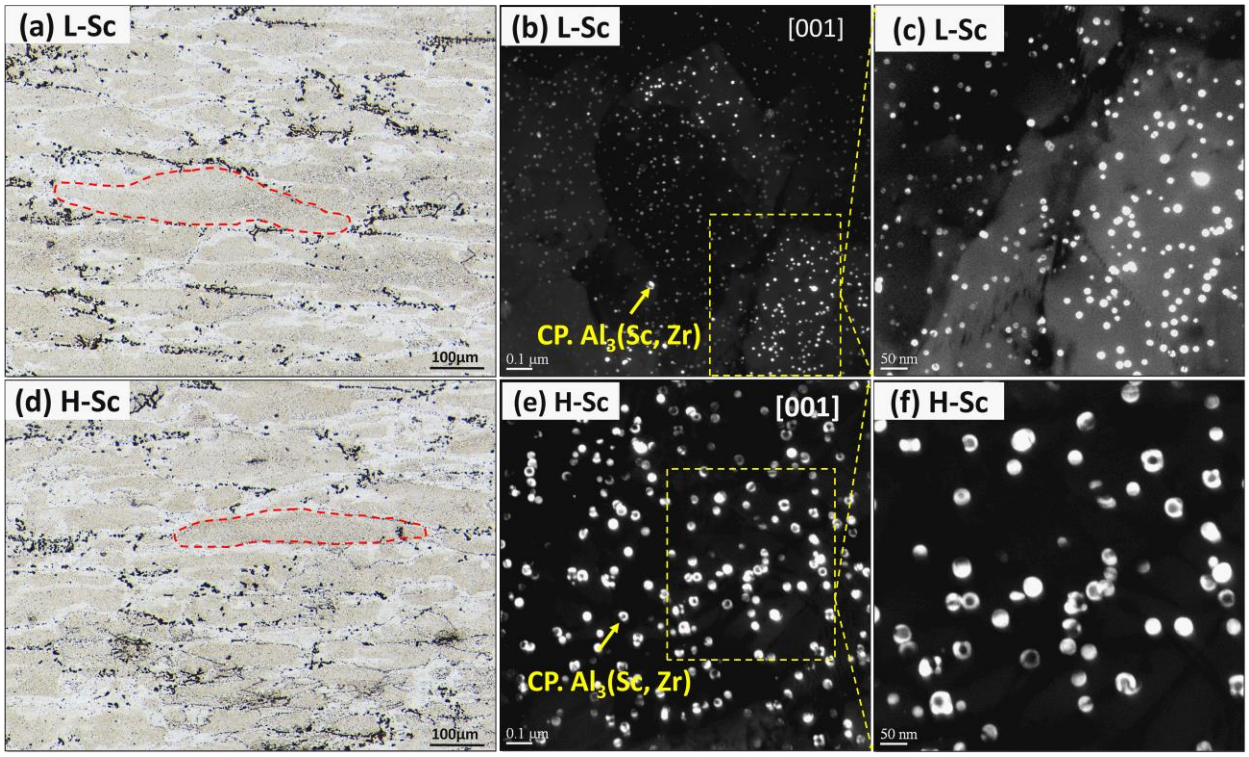

Figure 7: Typical optical microscopy images of the samples after hot rolling (a) L-Sc and (d) H-Sc samples. Dark-field TEM images showing the spherical $Al_3(Sc, Zr)$ precipitates after hot rolling (b, c) L-Sc and (e, f) H-Sc samples.

Fig. 8 presents a schematic overview of the evolution of the discontinuous and continuous precipitates during the thermomechanical process. Starting from the as-cast condition, the microstructure is similar between the base and L-Sc alloys, while a high density of fan- and line-shaped DCP formed at moving grain boundaries and extended to the grain interior in H-Sc alloy.

During the subsequent heat treatment, Mn-dispersoids are precipitated out in all three alloys but with decreasing number density in Sc-containing alloys. Meanwhile, continuous (CP) $Al_3(Sc,Zr)$ precipitates formed in both L-Sc and H-Sc alloy, but its volume was significantly higher in L-Sc alloy than H-Sc alloy. On the other hand, DCP was partially dissolved in H-Sc alloy. With further rolling and annealing, both Mn-dispersoids and CP $Al_3(Sc,Zr)$ precipitates underwent coarsening in experimental alloys, resulting in a decreased number density and increased size. Moreover, DCP was fully dissolved in H-Sc alloy, and the high Sc solutes from the dissolution of DCP in H-Sc accelerated the coarsening of the $Al_3(Sc,Zr)$ particles, leading to a larger size of CP $Al_3(Sc,Zr)$ in H-Sc alloy than L-Sc alloy through diffusion/growth mechanism

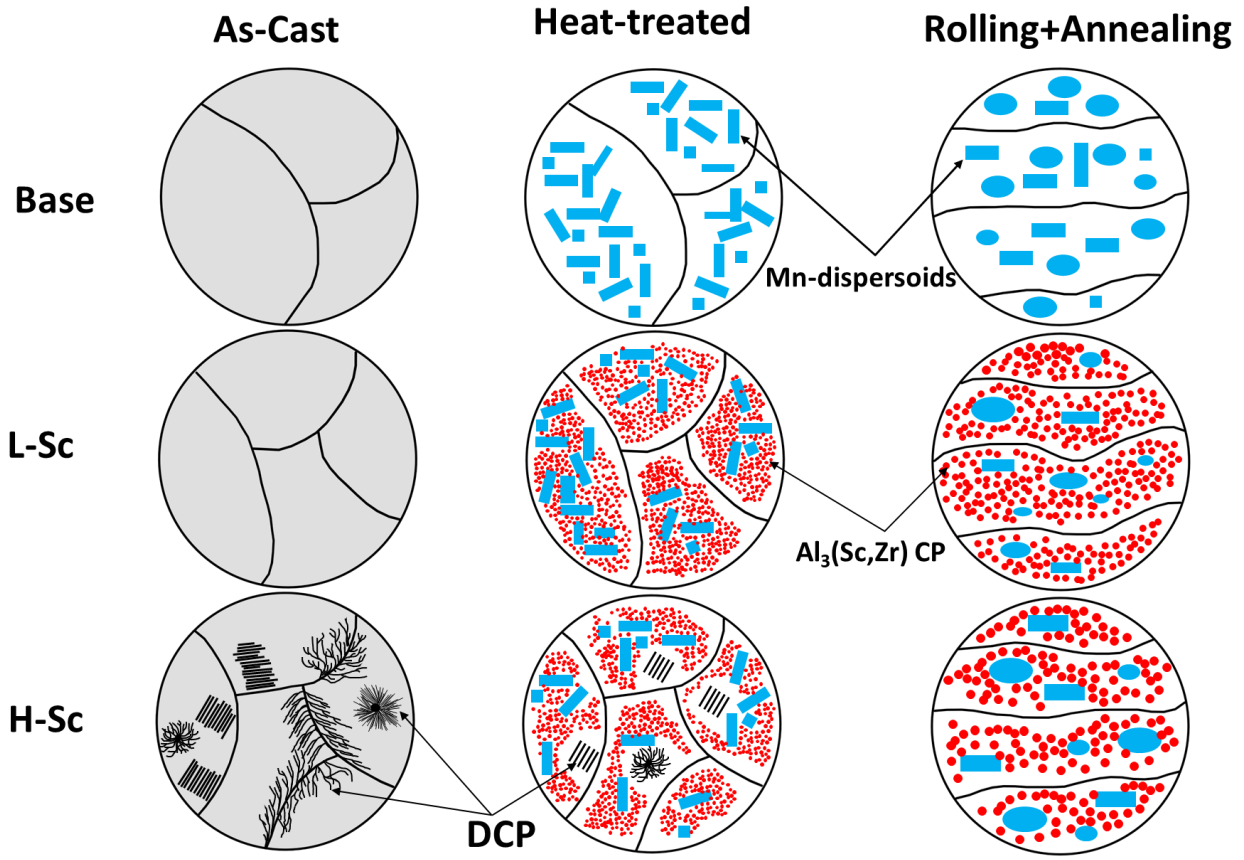

Figure 8: A schematic illustration on the evolution of Mn-dispersoids, discontinuous and continuous $Al_3(Sc,Zr)$ precipitates during thermomechanical process.

3.4 Tensile properties of hot rolled sheets

As summarized in Fig. 8, the evolution of Mn-dispersoids, CP and DCP precipitates varies with the addition of Sc. Therefore, it is expected to have different mechanical propertied related to the evolution of microstructure. Fig .9 displays the tensile properties of the hot-rolled samples tested at room temperature, considering that all the hot-rolled samples were annealed at 300 °C for 5 h to release the thermal stress induced by rolling. As shown in Fig. 9a, the stress level is increasing from base alloy to H-Sc and further to L-Sc, confirming the position contribution of Sc on

improving the mechanical properties. Fig. 9b shows the detailed tensile properties of the three alloys. It can be found that the tensile strength of the Sc-containing alloys was significantly higher than that of the base alloy owing to the additional strengthening effect of the spherical $Al_3(Sc,Zr)$ precipitates. The L-Sc alloy with a low Sc content exhibited the highest YS and UTS while the tensile properties deteriorated with an increase in the Sc content. For instance, the YS and UTS of the L-Sc alloy reached 298.4 and 494.3 MPa, respectively, showing an improvement of 30% in the YS and 8.2% in the UTS relative to the base alloy. On the other hand, the H-Sc alloy showed the YS and UTS values of 261 and 464.9 MPa, respectively, resulting in an improvement of 14% in the YS and 4.2% in the UTS as compared to the base alloy.

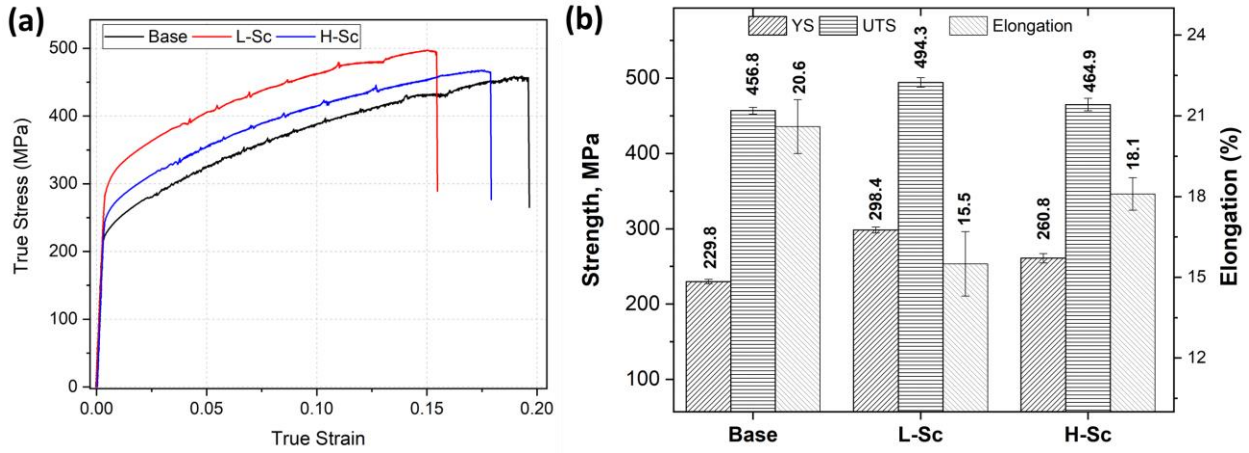

Figure 9: Typical true stress-strain curves of the hot-rolled samples (a), average tensile properties of all the three samples (b).

Generally, the improvement on the mechanical properties with the addition of Sc can be derived from the nano-sized CP $Al_3(ScZr)$ precipitates after rolling, which could pin the movement of dislocations and grain boundaries. As shown in Figs. 7 and 8, a high number density of CP $Al_3(ScZr)$ presented after rolling in Sc-containing alloys, providing the additional contribution on the mechanical properties relative to the base alloy.

On the other hand, the different mechanical properties between L-Sc and H-Sc alloys are closely related to the evolution of microstructure with Sc additions: The smaller size and higher density of CP $Al_3(Sc,Zr)$ precipitates (see Fig. 7b and Fig. 8) in L-Sc alloy contributed to its better tensile properties than those in H-Sc alloy. While the relatively low tensile properties of H-Sc alloy can be attributed to the following reasons: (1) During solidification, as shown in Fig. 1 and 8, a large number of rod-like DCP were formed, which consumed large amount of Sc and Zr in the solid solution, reducing the number of fine CP $Al_3(Sc,Zr)$ during heat treatment. (2) During the heat treatment process, fine CP $Al_3(Sc,Zr)$ precipitates could not be formed in the vicinity of the discontinuous precipitates (see Figs. 4 and 8) owing to the depletion of Sc and Zr in the surrounding area, resulting in a locally weakened strengthening effect. (3) Although the DCP dissolved completely during hot rolling (Fig, 8), the dissolved Sc in the solid solution could only promote

the coarsening of the CP Al_3(Sc,Zr) precipitates through diffusion/growth mechanism (Fig. 7), further weakening their strengthening effect [22].

4. Conclusions

In this study, we investigated the evolution of discontinuous/continuous Al_3(Sc,Zr) precipitation in an Al-Mg-MnAA5083 alloy during heat treatment and hot rolling as well as its impact on the tensile properties of the alloy. The following conclusions were drawn.

1) When a high amount of Sc (0.43 wt.%) was added, a large number of line- and fan-shaped structures were formed as discontinuous Al_3(Sc,Zr) precipitation during solidification. The length of these precipitates ranged from 500 to 860 nm. In the low-Sc alloy (0.15 wt.%), no such discontinuous precipitation was observed.
2) During the heat treatment process, two types of precipitates (Mn-bearing dispersoids and spherical Al_3(Sc,Zr) precipitates) were formed as the main strengthening phases. In the H-Sc alloy, the discontinuous Al_3(Sc,Zr) precipitates were partially dissolved, and their length decreased to 200–350 nm. The number density of the spherical Al_3(Sc,Zr) precipitates in the H-Sc alloy was much lower than that in the L-Sc alloy because the discontinuous precipitates consumed large amounts of Sc and Zr in the solid solution.
3) The microhardness of the heat-treated H-Sc alloy was lower than that of the heat-treated L-Sc alloy, which indicates that the discontinuous precipitates had a deleterious effect on the aging hardening response of the alloys.
4) During hot rolling, the discontinuous precipitates dissolved completely, and only the spherical Al_3(Sc,Zr) precipitates and Mn-bearing dispersoids existed in both the Sc-containing alloys. Both the precipitates and dispersoids underwent coarsening during hot rolling. However, the spherical Al_3(Sc,Zr) precipitates in the H-Sc alloy were lower in number density and larger insize than those in the L-Sc alloy.
5) The tensile properties were significantly improved in Sc-containing alloys, owing to the additional strengthening effect of spherical Al_3(Sc,Zr) precipitates. However, by increasing Sc content, the YS and UTS decreased, confirming the negative effect of discontinuous precipitates. The low Sc alloy exhibited the highest YS and UTS, showing an improvement of 30% in YS and 8.2% in UTS relative to the base alloy.

Acknowledgments

The authors would like to acknowledge the financial support from the Natural Sciences and Engineering Research Council of Canada (NSERC) and Rio Tinto Aluminum under the Grant No. CRDPJ 514651-17 through the Research Chair in Metallurgy of Aluminum Transformation at the University of Quebec at Chicoutimi.

References

[1] Z. Li, Z. Zhang, X.G. Chen, Improvement in the mechanical properties and creep resistance of Al-Mn-Mg 3004 alloy with Sc and Zr addition, Materials Science and Engineering A, 729 (2018) 196-207.
[2] X. Liu, Z. Guo, J. Xue, C. Zhu, P. Zhang, X. Li, Microstructures and mechanical properties of the Al-Cu-Sc alloys prepared by ultrasound-assisted molten salt electrolysis, Journal of Alloys and Compounds, 818 (2020) 152870-152870.
[3] Y. Wang, H. Liu, X. Ma, R. Wu, J. Sun, L. Hou, J. Zhang, X. Li, M. Zhang, Effects of Sc and Zr on microstructure and properties of 1420 aluminum alloy, Materials Characterization, 154 (2019) 241-247.
[4] S. Ikeshita, A. Strodahs, Z. Saghi, K. Yamada, P. Burdet, S. Hata, K.-i. Ikeda, P.A. Midgley, K. Kaneko, Hardness and microstructural variation of Al – Mg – Mn – Sc – Zr alloy, Micron, 82 (2016) 1-8.
[5] J. Jiang, F. Jiang, M. Zhang, Z. Tang, M. Tong, Recrystallization behavior of Al-Mg-Mn-Sc-Zr alloy based on two different deformation ways, Materials Letters, 265 (2020) 127455-127455.
[6] Y. Peng, S. Li, Y. Deng, H. Zhou, G. Xu, Z. Yin, Synergetic effects of Sc and Zr microalloying and heat treatment on mechanical properties and exfoliation corrosion behavior of Al-Mg-Mn alloys, Materials Science and Engineering A, 666 (2016) 61-71.
[7] C.B. Fuller, D.N. Seidman, D.C. Dunand, Mechanical properties of Al (Sc, Zr) alloys at ambient and elevated temperatures, Acta Materialia, 51 (2003) 4803-4814.
[8] S.M. Anijdan, D. Kang, N. Singh, M. Gallerneault, Precipitation behavior of strip cast Al–Mg–0.4 Sc–0.15 Zr alloy under single and multiple-stage aging processes, Materials Science and Engineering: A, 640 (2015) 275-279.
[9] D.N. Seidman, E.A. Marquis, D.C. Dunand, Precipitation strengthening at ambient and elevated temperatures of heat-treatable Al (Sc) alloys, Acta Materialia, 50 (2002) 4021-4035.
[10] S.a. Zhou, Z. Zhang, M. Li, D. Pan, H. Su, X. Du, P. Li, Y. Wu, Effect of Sc on microstructure and mechanical properties of as-cast Al-Mg alloys, Materials and Design, 90 (2016) 1077-1084.
[11] C.B. Fuller, J.L. Murray, D.N. Seidman, Temporal evolution of the nanostructure of Al(Sc ,Zr) alloys:Part I -Chemical compositions of Al3(Sc1-xZrx) precipitates, Acta Materialia, 53 (2005) 5401-5413.
[12] J. Lai, Z. Zhang, X.G. Chen, The thermal stability of mechanical properties of Al-B 4C composites alloyed with Sc and Zr at elevated temperatures, Materials Science and Engineering A, 532 (2012) 462-470.
[13] A.K. Lohar, B. Mondal, D. Rafaja, V. Klemm, S.C. Panigrahi, Microstructural investigations on as-cast and annealed Al-Sc and Al-Sc-Zr alloys, Materials Characterization, 60 (2009) 1387-1394.
[14] J. Røyset, N. Ryum, Scandium in aluminium alloys, International Materials Reviews, 50 (2005) 19-44.
[15] J. Røyset, N. Ryum, Kinetics and mechanisms of precipitation in an Al-0.2wt.% Sc alloy, Materials Science and Engineering A, 396 (2005) 409-422.
[16] Y. Sun, Q. Pan, Y. Luo, S. Liu, W. Wang, J. Ye, Y. Shi, Z. Huang, S. Xiang, Y. Liu, The effects of scandium heterogeneous distribution on the precipitation behavior of Al3(Sc, Zr) in aluminum alloys, Materials Characterization, 174 (2021).
[17] Q. Dong, A. Howells, D.J. Lloyd, M. Gallerneault, V. Fallah, Effect of solidification cooling rate on kinetics of continuous/discontinuous Al3(Sc,Zr) precipitation and the subsequent age-hardening response in cold-rolled AlMgSc(Zr) sheets, Materials Science and Engineering A, 772 (2020) 138693-138693.
[18] S. Lathabai, P.G. Lloyd, The effect of scandium on the microstructure, mechanical properties and weldability of a cast Al-Mg alloy, Acta Materialia, 50 (2002) 4275-4292.
[19] W. Zhang, Y. Wu, H. Lu, G. Lao, K. Wang, Y. Ye, P. Li, Discontinuous Precipitation of Nano-Al3Sc Particles in Al-Sc Alloy and its Effect on Mechanical Property, International Journal of Nanoscience, 19 (2020).
[20] A. Norman, P. Prangnell, R. McEwen, The solidification behaviour of dilute aluminium–scandium alloys, Acta materialia, 46 (1998) 5715-5732.

[21] N.B. Hopkins, A. M, Constitution and age hardening of Al-Sc alloys, Journal of Materials Science, 20 (1985) 2861-2867.
[22] A.K. Lohar, B.N. Mondal, S.C. Panigrahi, Influence of cooling rate on the microstructure and ageing behavior of as-cast Al–Sc–Zr alloy, Journal of Materials Processing Tech., 210 (2010) 2135-2141.
[23] A. Mochugovskiy, V. Levchenko, N.Y. Tabachkova, W. Mufalo, V. Portnoy, Precipitation behavior of L12 Al3Zr phase in Al-Mg-Zr alloy, Materials Characterization, 139 (2018).
[24] D.O. P. B. Prangnell, S. W. M, Discontinuous precipitation in high Li content Al-Zr alloys, Acta Metallurgica Et Materialia, 42 (1994) 419-433.
[25] A.Y. Algendy, K. Liu, X.G. Chen, Evolution of dispersoids during multistep heat treatments and their effect on rolling performance in an Al-5 % Mg-0 . 8 % Mn alloy, Materials Characterization, 181 (2021) 111487-111487.
[26] S.M. Allen, Foil thickness measurements from convergent-beam diffraction patterns, Philos. Mag, A 43 (1981) 325-335.
[27] D.B. Williams, E.P. Butler, Grain boundary discontinuous precipitation reactions, International Metals Reviews, 4590 (2013) 153-183.
[28] Y.W. Riddle, T.H. Sanders, A Study of Coarsening , Recrystallization , and Morphology of Microstructure in Al-Sc- (Zr) - (Mg) Alloys, METALLURGICAL AND MATERIALS TRANSACTIONS A, 35 A (2004) 341-350.
[29] A.G. Mochugovskiy, A.V. Mikhaylovskaya, N.Y. Tabachkova, V.K. Portnoy, The mechanism of L12 phase precipitation, microstructure and tensile properties of Al-Mg-Er-Zr alloy, Materials Science and Engineering A, 744 (2019) 195-205.
[30] E. Hornbogen, Systematics of the Cellular Precipitation Reactions, Metallurgical transactions. A, 3 (1972) 2717-2727.
[31] E.A. Marquis, D.N. Seidman, Nanoscale structural evolution of Al 3 Sc precipitates in Al(Sc) alloys, Acta Materialia, 49 (2001) 1909-1919.
[32] D. Tsivoulas, J. Robson, Heterogeneous Zr solute segregation and Al3Zr dispersoid distributions in Al–Cu–Li alloys, Acta Materialia, 93 (2015) 73-86.
[33] W. Lefebvre, F. Danoix, H. Hallem, B. Forbord, A. Bostel, K. Marthinsen, Precipitation kinetic of Al3(Sc, Zr) dispersoids in aluminium, Journal of Alloys and Compounds, 470 (2009) 107-110.
[34] A.G. Mochugovskiy, A.V. Mikhaylovskaya, Comparison of precipitation kinetics and mechanical properties in Zr and Sc-bearing aluminum-based alloys, Materials Letters, 275 (2020) 128096-128096.
[35] Y. Du, Y.A. Chang, B. Huang, W. Gong, Z. Jin, H. Xu, Z. Yuan, Y. Liu, Y. He, F.Y. Xie, Diffusion coefficients of some solutes in fcc and liquid Al: Critical evaluation and correlation, Materials Science and Engineering A, 363 (2003) 140-151.
[36] A.V. Mikhaylovskaya, A.G. Mochugovskiy, V.S. Levchenko, N.Y. Tabachkova, W. Mufalo, V.K. Portnoy, Precipitation behavior of L12 Al3Zr phase in Al-Mg-Zr alloy, Materials Characterization, 139 (2018) 30-37.
[37] E.a. Marquis, D.N. Seidman, Coarsening Kinetics of Nanoscale Al-3Sc Precipitates in an Al-Mg-Sc Alloy, Acta Mater., 53 (2005) 4259-4268.
[38] K. Yan, Z. Chen, W. Lu, Y. Zhao, W. Le, S. Naseem, Nucleation and growth of Al3Sc precipitates during isothermal aging of Al-0 . 55 wt % Sc alloy, Materials Characterization, 179 (2021) 111331-111331.
[39] M. Cabibbo, E. Evangelista, M. Vedani, Influence of severe plastic deformations on secondary phase precipitation in a 6082 Al-Mg-Si alloy, Metallurgical and Materials Transactions A, 36 (2005) 1353-1364.
[40] I. Lomaev, E. Elsukov, On the analysis of the mechanisms of the strain-induced dissolution of phases in metals, PHYSICS OF METALS AND METALLOGRAPHY C/C OF FIZIKA METALLOV I METALLOVEDENIE, 102 (2006) 186.